

## Theory and computational study of electrophoretic ion separation and focusing in microfluidic channels

Oleksiy V. Klymenko<sup>a</sup>, Christian Amatore<sup>a</sup>, Wen Sun<sup>b</sup>, Yong-Liang Zhou<sup>b</sup>,  
Zhao-Wu Tian<sup>b</sup>, Irina Svir<sup>a</sup>

<sup>a</sup>Ecole Normale Supérieure, Département de Chimie, UMR 8640  
24 rue Lhomond, 75005 Paris, France  
irina.svir@ens.fr

<sup>b</sup>Xiamen University, Department of Chemistry  
State Key Laboratory for Physical Chemistry of Solid Surfaces  
361005 Xiamen, China

**Received:** 12 October 2012 / **Revised:** 2 November 2012 / **Published online:** 22 November 2012

**Abstract.** In this work we describe the theory and 2D simulation of ion separation and focusing in a new concept of microfluidic separation device. The principle of the method of ion focusing is classical in the sense that it consists in opposing a hydrodynamic transport ensured by the solution flow to an electrophoretic driving force so that any ionic sample results poised within the microchannel at the point where the two forces equilibrate. The originality of the concept investigated here relies on the fact that thanks to the use of an ion-conducting membrane of variable thickness in electrical contact with the channel the electrophoretic force is varied continuously all along the channel length. Similarly, changing the geometric shape of the membrane allows a facile optimization of the device separation and focusing properties.

**Keywords:** electrophoresis, analytical separation, ion-conducting membranes, 2D simulation.

### 1 Introduction

The development and the present facile access to microfabrication devices has led to great improvements in analytical separative devices [1–11] in particular concerning those involving a wide range of electrically driven applications, e.g., capillary electrophoresis [12–17], electrokinetic chromatography [18–22], gel electrophoresis [23–29], etc. Implementation of these techniques within microfluidic channels has allowed spectacular progress in biological and chemical analyses (see, for example, [30, 31]). However, albeit many advantages have been demonstrated over conventional methods, the shorter lengths of microchannel separative devices create intrinsic difficulties concerning absolute separation efficiencies. Indeed, due to the small cross-sections of electrically driven microfluidic separative microchannels the current densities are high and must be limited when the microchip material cannot radiate easily the important Joule effect [1]. This in turn limits the magnitude of the separation electrical voltage, hence the absolute separation efficiency.

A second limitation, valid for any separative microdevice, is related to the fact that characterization of the targeted analyte generally requires that sophisticated detection means (e.g., mass spectrometry) [32–37] are connected to the exit of the separation microchannel, thus reproducing the same constraints as in classical separation methods but with a higher difficulty since the amount of analyte is minute.

Recent experiments have demonstrated that another strategy may be implemented with success when the analyte is charged [38–46]. This amounts to focusing a targeted analyte by opposing two means of transport within the separative microchannel: a constant one-direction solution flow of average velocity  $v_{\text{avg}}$  which carries the analyte and a counter-direction electrokinetic force [47–58] (which depends on the analyte charge,  $q = z|e|$ , and its diffusion coefficient,  $D$ ) whose intensity increases continuously along the microchannel separation length. Under such conditions, analytes with given product  $zD$  result poised within the microchannel at a distance,  $x_0$ , such as  $zD = (RT/F)v_{\text{avg}} / (d\varphi/dx)_{x_0}$  where  $(d\varphi/dx)$  is the electrical potential gradient imposed at any point  $x$  of a channel.

To obtain a constant flow rate the microchannel must have a constant cross-section. Therefore, in order to create and adjust at will the gradient  $(d\varphi/dx)$  one needs to divert part of the current flow along the microchannel length [59, 60]. This may be performed in a continuous mode by carrying out the separation in the presence of an excess of supporting electrolyte and implementing an ion-conducting membrane with nanopores (e.g., Nafion<sup>®</sup>) with variable thickness into one of the channel walls as represented schematically in Fig. 1(a). Note that a conceptually analogous approach in which the electrical field experiences a continuous gradient within the microchannel has been recently proposed [61–64]. However, both approaches differ essentially in the sense that in this previous work the variable electrophoretic driving force results from paired electrochemical reactions occurring at each end of a bipolar electrode inserted in the channel. This imposes a strong localization of the electrophoretic force gradient near each end of the bipolar electrode while in the present concept the gradient variations are spread at will over the whole channel length.

Under the conditions of Fig. 1(a), at any given position within the microchannel, the current flow faces two parallel resistances representative of each ionic transport mode, one through the solution and the other through the membrane as sketched in Fig. 1(b) for an element  $dx$  of the channel length. If the membrane nanopores are too small for allowing the analytes of interest to be carried through the membrane, they will be transported within the solution while experiencing a gradient of the electrical force which may then oppose more and more efficiently to the counter-transport by the solution flow. The ensuing decrease in transport rate along the electrical gradient proceeds up to the point when the selected analyte necessarily stops and may then be detected by any imaging technique such as fluorescence.

The main goal of this work is to investigate the theoretical aspects of this separation method and evidence by a series of 2D-simulations how such devices perform in particular when two analytes need to be focused at two different points along the microchannel length. For this purpose we will consider that the ion-conducting membrane has been deposited so that its thickness varies linearly along the channel length (Fig. 1a) but evi-

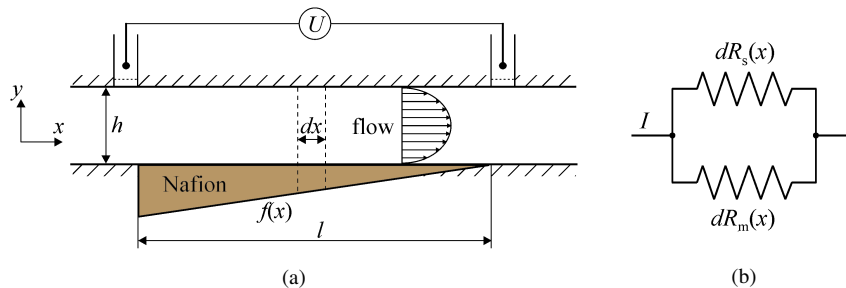


Fig. 1. (a) Schematic description of the focusing microchannel system geometry; (b) equivalent electrical circuit of a vertical slice of thickness  $dx$  of the microchannel shown in (a).

Other shapes may be implemented experimentally or in the simulations to test and predict if this would lead to better separation efficiencies under particular circumstances. Indeed, the present model involving a combination between analytical formulations and simulations is sufficiently versatile to test any configuration, hence to allow optimization of the device towards a particular case of interest.

A computer program written by the authors allows performing 2D simulations for different experimental situations in order to optimize the focusing properties. The simulation can readily account for both parabolic and constant (electroosmotic) flows and can be easily modified to cover more complicated situations.

## 2 Theory

### 2.1 Physico-chemical model

Consider a flow channel as depicted in Fig. 1(a) of height  $h$  and lateral width  $w$  (in the direction perpendicular to the cross-section in Fig. 1(a);  $w \gg h$ ). The solution within the channel is supposed to flow due to an external pressure gradient. In order to create conditions for separating charged particles according to their effective charge an electric field is generated within the channel using two electrodes located at a distance  $l$  from each other in the direction of the flow ( $l \gg h$  and  $l \gg w$ ). The potential difference between these electrodes is  $U = V(x = L) - V(x = 0)$  and it is assumed that the electrical equipotential planes are vertical within the part of interest of the channel, viz. the field is planar and parallel to the channel length. Finally, for simplification we consider here that the electroosmotic drive due to the electrical field is negligible and that the main drive of electrochemical origin is by electrophoresis (note that in the experiments shown here the solution hydrodynamic flow is ensured only by electroosmotic forces due to the configuration of the experimental set-up). The theory developed below may easily be expanded to consider electroosmotic forces [65–67] and streaming potential [68] if this revealed of importance.

This electric field induces an electric current due to the movement of charged analytes and inert ions of supporting electrolyte with respect to the flowing solution. Additionally,

the ionic current may also pass through a layer of ion-conducting membrane which is in electrical contact with one of the channel walls and has a varying thickness described by a function  $f(x)$ . Thus the overall conductance of the solution and the membrane layer as a function of the coordinate  $x$  may be adjusted to achieve the required potential (field) distribution. Note that the exact positioning of the membrane vis-a-vis the microchannel is irrelevant within the level of approximation used in this work provided that at least one wall of the channel is electrically connected to the membrane.

Consider a vertical slice (of thickness  $dx$ ) of the channel together with the ion-conducting wall (see Fig. 1(a)). The overall electric current  $I$  flowing through the system is distributed between the solution and ion-conducting film according to their relative resistances. The channel slice can thus be represented by an equivalent circuit shown in Fig. 1(b) where  $dR_s(x)$  represents the resistance of the elementary solution slice and  $dR_m(x)$  is the elementary resistance of the ion-conducting membrane slice at a lateral position  $x$ .

Denoting the ionic conductivities of the solution and membrane as  $\gamma_s$  and  $\gamma_m$  (which we assume for now to be constant), respectively, the elementary resistances may be expressed as [69]:

$$dR_s(x) = \frac{1}{\gamma_s} \frac{dx}{hw}, \quad (1)$$

$$dR_m(x) = \frac{1}{\gamma_m} \frac{dx}{wf(x)}. \quad (2)$$

The overall resistance of the channel slice is then:

$$dR(x) = \frac{dx}{w(\gamma_s h + \gamma_m f(x))}. \quad (3)$$

From the Ohm's law the potential drop at this elementary channel slice is  $d\varphi = IdR$ , so that the potential distribution along the channel is described by the following integral:

$$\varphi(x) = I \int_0^x \frac{dx}{w(\gamma_s h + \gamma_m f(x))}. \quad (4)$$

Noting that the potential drop along the whole distance between the electrodes is  $\varphi(l) = U$ , one can eliminate the current  $I$  and channel width  $w$  from (4) to obtain:

$$\varphi(x) = \frac{U \int_0^x \frac{dx}{w(\gamma_s h + \gamma_m f(x))}}{\int_0^l \frac{dx}{w(\gamma_s h + \gamma_m f(x))}}. \quad (5)$$

For example, in the case of a wedge-shaped ion-conducting layer (i.e. with  $f(x)$  varying linearly with a wedge-slope  $k$  and from a zero value at  $x = l$  as shown in Fig. 1(a)

the ensuing potential distribution along the channel is logarithmic:

$$f(x) = k(l - x), \quad (6)$$

$$\varphi(x) = U \frac{\ln\left(\frac{\gamma_s h + \gamma_m k(l-x)}{\gamma_s h + \gamma_m k l}\right)}{\ln\left(\frac{\gamma_s h}{\gamma_s h + \gamma_m f(x)}\right)}. \quad (7)$$

This is represented in Fig. 2 for different values of the wedge-slope  $k$  and shows that the potential variations and those of electrical field may be adjusted at will simply by changing the wedge-slope of the membrane. This evidences the great versatility of the present concept.

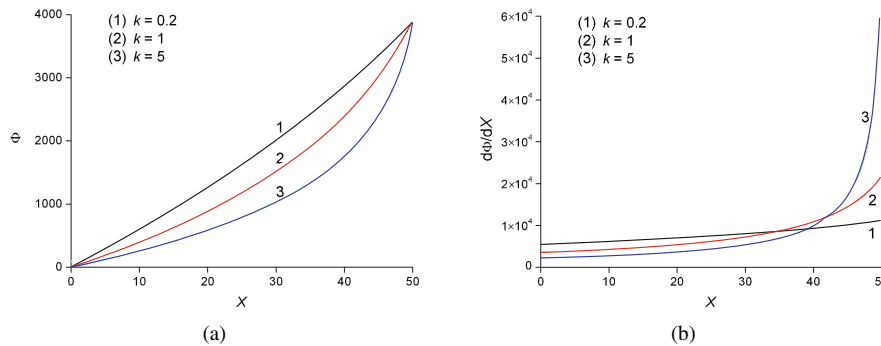


Fig. 2. Dimensionless electric potential  $\Phi$  (a) and field  $d\Phi/dX$  (b) variations along the channel length for three different wedge slopes as indicated by the values of  $k$  on the curves.  $X = x/h$ ,  $\Phi = F\varphi/RT$ . Variations are shown for  $\gamma_s = 10^{-3} \text{ Ohm}^{-1} \text{ cm}^{-1}$ ,  $\gamma_m = 10^{-4} \text{ Ohm}^{-1} \text{ cm}^{-1}$  and  $L = l/h = 50$ .

Equation (5) was obtained under the assumption of constant conductivities of the solution and membrane. However, when this is not the case (viz., when there is a non-uniform distribution of ionic species throughout the solution and membrane due to ion exchange between them) this expression needs to be modified only slightly. Indeed, the resistances (1) and (2) of elementary vertical slices of the solution and membrane layer in this case become:

$$dR_s(x) = \frac{dx}{w \int_0^h \gamma_s(x, y) dy}, \quad (8)$$

$$dR_m(x) = \frac{dx}{w \int_0^{f(x)} \gamma_m(x, y) dy}, \quad (9)$$

where  $\gamma_s(x, y)$  and  $\gamma_m(x, y)$  are location-dependent conductivities of the solution and membrane layer, respectively. Therefore the integrand in both the numerator and denominator of (5) becomes:

$$w dR(x) = \frac{dx}{\int_0^h \gamma_s(x, y) dy + \int_0^{f(x)} \gamma_m(x, y) dy}, \quad (10)$$

and the potential distribution (5) may be rewritten as:

$$\varphi(x) = U \frac{\int_0^x dR(x)}{\int_0^l dR(x)}. \quad (11)$$

If the solution contains a target molecule (or particle) with the effective charge  $q$  the electric field within the channel will exert a force on it equal to:

$$F(x) = -q \frac{d\varphi(x)}{dx}. \quad (12)$$

When this force is opposite in direction to the hydrodynamic force pushing the molecule in the direction of the flow, and provided that the channel is long enough, there is necessarily a position,  $x_0$ , along the channel where these two forces equilibrate each other, which corresponds to the point where the analyte will accumulate. Equivalently, the analyte will stop when its hydrodynamic velocity is exactly compensated by the velocity imposed by the electric field. Then from the definition of mobility ( $u = v/E$ , where  $v$  is the speed of the molecule and  $E$  is the field) and the Einstein–Smoluchowski relation ( $u = |z|FD/RT$ , where  $z = q/|e|$  and  $D$  is the diffusion coefficient of the molecule) one readily obtains the relative speed of the charged analyte imposed within the flowing solution by the electrical field [70]:

$$v(x) = \frac{zFD}{RT} \frac{d\varphi(x)}{dx}. \quad (13)$$

If for simplification we consider that the whole solution flows hydrodynamically at its average velocity,  $v_{\text{avg}}$ , the charged analyte has an absolute velocity (i.e., vs. the channel walls) given by  $v_{\text{avg}} - v(x)$  (note that this is essentially correct for an electroosmotic solution flow). This shows that any charged analyte will stop at the position  $x_0$  such that

$$\frac{zFD}{RT} \left[ \frac{d\varphi(x)}{dx} \right]_{x_0} = v_{\text{avg}}. \quad (14)$$

A more exact determination of the position of the focused species sample and its width requires implementing the exact shape of the flow velocity. This will be performed below on the basis of the full analysis of mass transport conditions within the channel and of simulations for the solutions of the ensuing equations.

## 2.2 Mathematical model

The actual distribution of the molecules is described by the following mass-transport equation [13]:

$$\frac{\partial c}{\partial t} = D \left( \frac{\partial^2 c}{\partial x^2} + \frac{\partial^2 c}{\partial y^2} \right) + \frac{zFD}{RT} c \frac{d^2 \varphi}{dx^2} - \left( v_x - \frac{zFD}{RT} \frac{d\varphi}{dx} \right) \frac{\partial c}{\partial x}, \quad (15)$$

where  $v_x(y)$  is the flow profile function (e.g., parabolic Poiseuille flow) and the formulation of Eq. (15) takes into account that the potential distribution is independent of the

coordinate  $y$ . Note that the consideration of a constant flow profile (viz., corresponding to electroosmotic drive) simplifies the problem at hand by practically reducing it to a single spatial dimension along the channel axis. Therefore we do not consider this situation here and focus below on the parabolic hydrodynamic flow.

It is assumed that initially a plug sample of analyte is injected at some axial position  $x_s$  (which lies either within the separation device or upstream of it) and has a width  $w_s$ . Hence, at  $t = 0$  the concentration  $c = c_0$  for  $x_s - w_s/2 \leq x \leq x_s + w_s/2$  and  $0 \leq y \leq h$  and is zero elsewhere.

There is no interaction of the target species with the channel walls, so

$$\frac{\partial c}{\partial y} = 0 \quad \text{for } y = 0 \text{ and } y = h. \quad (16)$$

Since the sample has a finite size, at large distances from the separation device the concentration remains zero at all times:

$$c = 0 \quad \text{for } x = \pm\infty, \quad 0 \leq y \leq h. \quad (17)$$

Let us introduce the following dimensionless variables and parameters:

$$\begin{aligned} \tau &= \frac{Dt}{h^2}, \quad X = \frac{x}{h}, \quad Y = \frac{y}{h}, \quad C = \frac{c}{c_0}, \\ \Phi &= \frac{F}{RT}\varphi, \quad V_X = \frac{v_x h}{D}, \quad Pe = \frac{v_{\text{avg}} h}{D}. \end{aligned} \quad (18)$$

Then the mass transport equation (15) rewrites as

$$\frac{\partial C}{\partial \tau} = \frac{\partial^2 C}{\partial X^2} + \frac{\partial^2 C}{\partial Y^2} + zC \frac{d^2 \Phi}{dX^2} - \left( V_X - z \frac{d\Phi}{dX} \right) \frac{\partial C}{\partial X}, \quad (19)$$

and the initial condition becomes

$$C = 1 \quad \text{for } X_s - \frac{W_s}{2} \leq X \leq X_s + \frac{W_s}{2}, \quad 0 \leq Y \leq 1, \quad (20)$$

where the upper-case symbols represent the normalized parameters corresponding to lower-case ones. Boundary conditions (16), (17) retain their form in the normalized terms and therefore are not repeated here.

Note that the species is theoretically ‘‘focused’’ only at large times, i.e., when  $\tau \rightarrow \infty$ , which corresponds to steady state conditions, though the plots shown in Fig. 3(e) establish that this is met asymptotically within reasonable times. In this case the initial position of the sample injection is not important and the resulting concentration distribution depends only on five dimensionless parameters: the charge of the species  $q = z|e|$ , the normalized channel length  $L$ , the normalized initial sample width  $W_s$  at the point of injection, the Peclet number of the carrier flow,  $Pe$ , and the normalized potential distribution along the channel  $\Phi(X)$  (compare with Fig. 2).

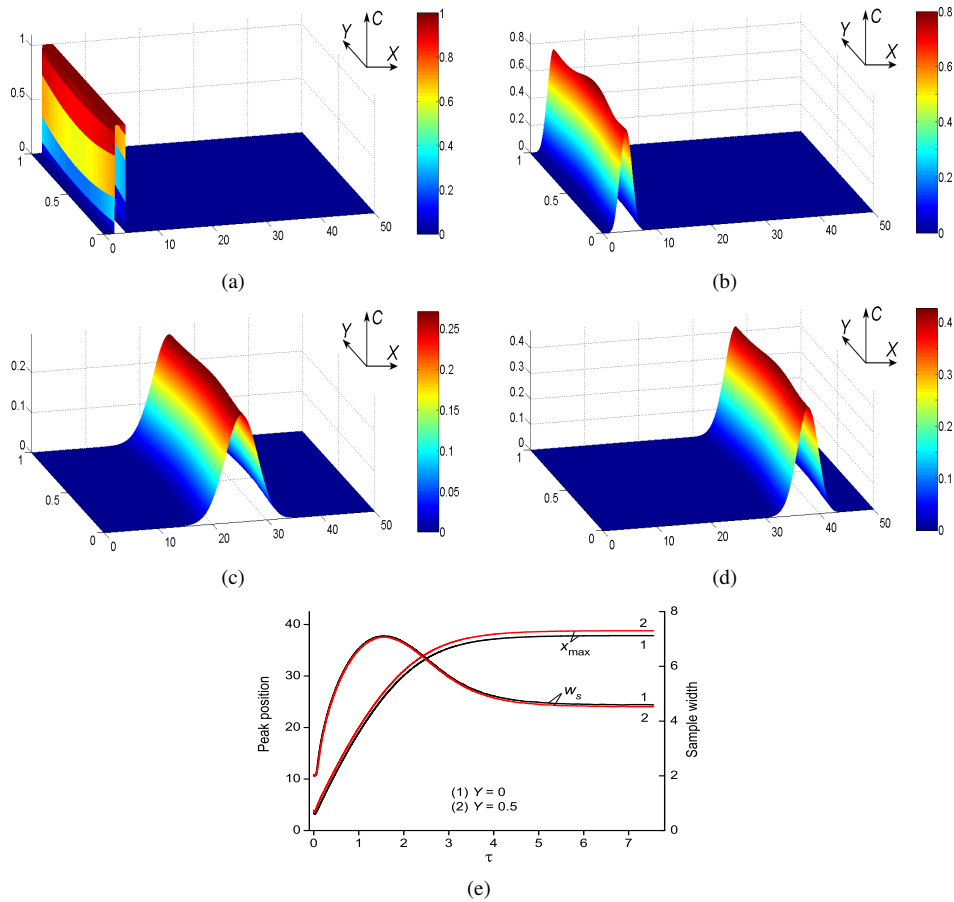


Fig. 3. Electrophoretic focusing of a single species for  $Pe = 30$  and  $\Psi = FU/RT = 1194.66$  (real parameter values:  $U = 30$  V,  $v_{avg} = 0.03$  cm s $^{-1}$ ). Simulated normalized concentrations shown in 3D after different durations: (a)  $\tau = 0$ ; (b)  $\tau = 0.1$ ; (c)  $\tau = 1.5$  (corresponds to maximum sample width); (d)  $\tau = 7.5$ . See text for other parameter values. In (e) are shown the variations of the maximum and half-width of the sample distribution at the centre of the channel or near its floor.

### 3 Simulation results

#### 3.1 Time-evolution of a single species containing sample

Figures 3–6 show normalized concentration distributions for a sample containing a single charged molecule simulated for a linear ion-conducting layer with a wedge-slope (unless otherwise stated)  $k = 1$  (see Eq. (7)) and the following dimensioned parameter values:  $h = 0.01$  cm,  $l = 0.5$  cm,  $D = 10^{-5}$  cm $^2$ s $^{-1}$ ,  $z = 1$ ,  $\gamma_s = 10^{-3}$  Ohm $^{-1}$ cm $^{-1}$ ,

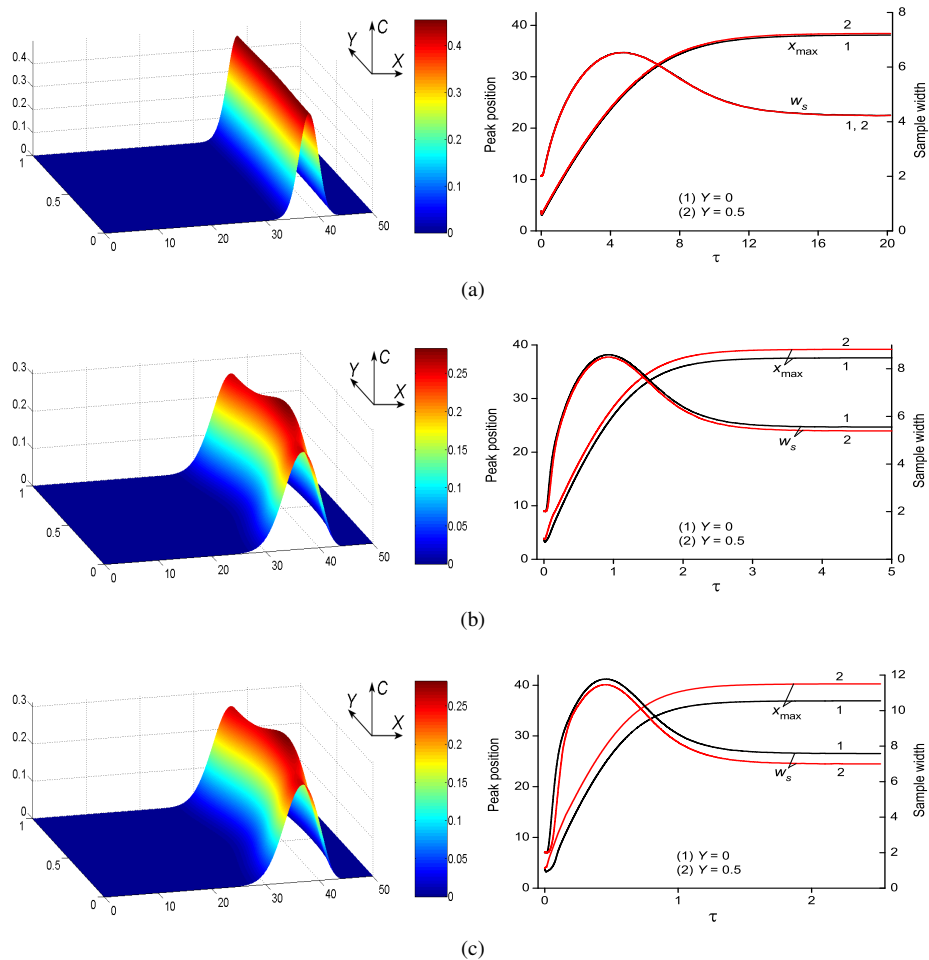


Fig. 4. Simulated focused normalized concentrations in 3D for three different combinations of the Peclet number: (a)  $Pe = 10$  ( $v_{\text{avg}} = 0.01 \text{ cm s}^{-1}$ ); (b)  $Pe = 50$  ( $v_{\text{avg}} = 0.05 \text{ cm s}^{-1}$ ) and (c)  $Pe = 100$  ( $v_{\text{avg}} = 0.1 \text{ cm s}^{-1}$ ), and the voltage applied between the two electrodes: (a)  $\Psi = 389.2$  ( $U = 10 \text{ V}$ ); (b)  $\Psi = 1946.1$  ( $U = 50 \text{ V}$ ) and (c)  $\Psi = 3892.2$  ( $U = 100 \text{ V}$ ). See text for other parameter values.

$\gamma_{\text{m}} = 10^{-4} \text{ Ohm}^{-1}\text{cm}^{-1}$ ,  $T = 298.15 \text{ K}$ ,  $w_{\text{s}} = 0.02 \text{ cm}$  (dimensionless channel length  $L = 50$ , dimensionless initial sample width  $W_{\text{s}} = 2$ ). In each case simulated hereafter the centre of the sample injection is arbitrarily set at the dimensionless position  $X_{\text{s}} = 2.5$ . The values of applied potential  $U$  and average flow velocity  $v_{\text{avg}}$  are given in each figure caption together with corresponding dimensionless parameters.

All the geometrical and physicochemical parameter values correspond to real experiments performed by the Xiamen group.

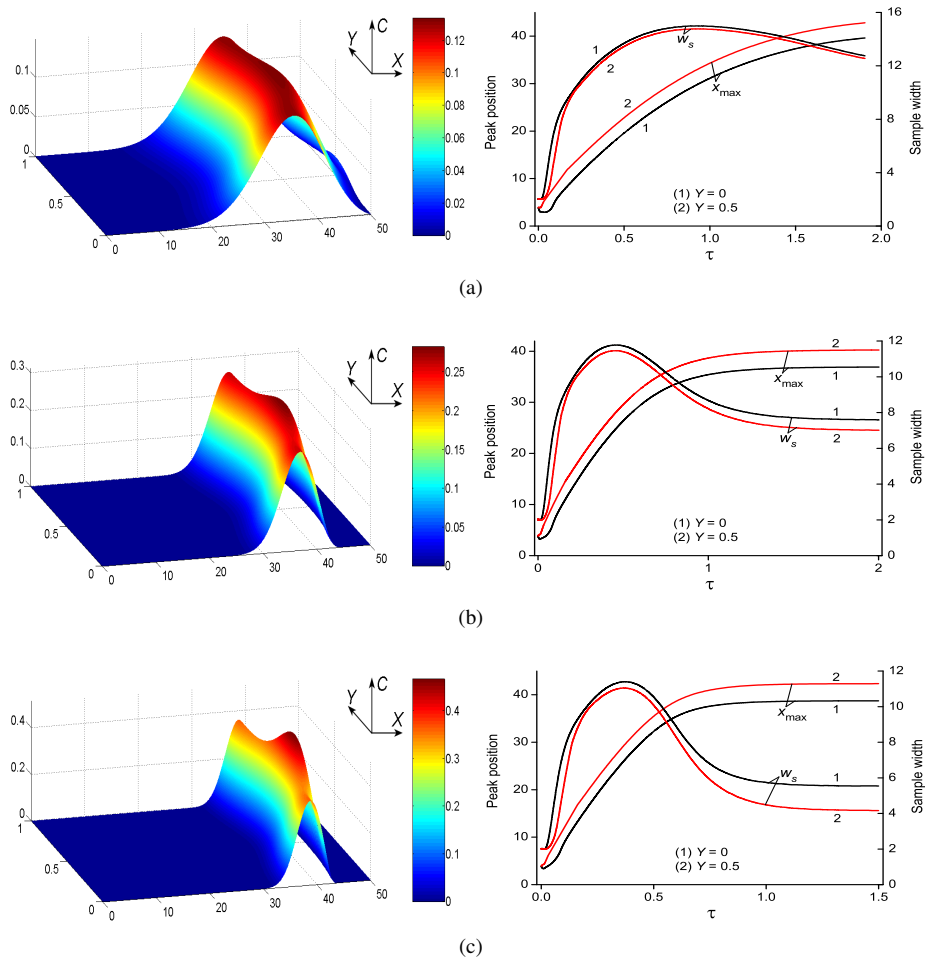


Fig. 5. Simulated normalized concentration distributions for  $Pe = 100$  and  $\Psi = 3892.2$  for different slopes of the wedge-shaped ion-conducting layer: (a)  $k = 0.2$ ; (b)  $k = 1$ ; (c)  $k = 5$ . See text for other parameter values.

The plots in Figs. 3–6 show that at short times the concentration distribution spreads diffusively and moves downstream (i.e., to the right in all figures) being almost unaffected by the electrophoretic forces.

This is evidenced in Fig. 3(e) where one observes that the sample concentration moves initially linearly with time. At long times (Fig. 3(e)) the sample approaches the point where the electrophoretic velocity becomes roughly equal to the average hydrodynamic velocity so that the sample displacement is gradually slowed down and eventually stopped. Note that since the solution hydrodynamic flow varies across  $y$ , the point at which the analyte concentration distribution in the center of the channel (viz., at  $y = h/2$ ,

i.e.,  $Y = 0.5$ ) is stopped and that at which it stops near the channel wall (viz., at  $y = 0$  or  $y = h$ , i.e.,  $Y = 0$  or  $Y = 1$ ) must differ. This is evidenced in Fig. 3(e) by comparing the  $X_{\max}$  positions at  $Y = 0.5$  and  $Y = 0$  or by examining the variations of the sample half-width variations ( $W_s$ ) with time again at  $Y = 0.5$  and  $Y = 0$ . These latest plots also establish that while the sample starts to enlarge its half-width due to diffusion over the range of time in which it progresses almost linearly along the channel length, as soon as the electrophoretic contribution becomes sufficiently important the sample is progressively focused, i.e. its concentration distribution becomes narrower than when it was traveling at intermediate times. Thus, not only the sample is ultimately poised at a given position within the channel, but it is also focused so as to eliminate part of the effect of diffusional spreading incurred during its initial travel within the channel.

More precisely this focusing property of the present device (viz., the width and shape of the focused concentration distribution obtained at steady state) depends on the intensities of flow and the electric field. This is demonstrated in Fig. 4 for three different combinations of the Peclet number ( $Pe = 10, 50$  and  $100$ ) and the voltage applied between the two electrodes ( $U = 10$  V,  $50$  V,  $100$  V, which correspond to dimensionless values  $\Psi = FU/RT = 389.2, 1946.1$  and  $3892.2$ , respectively). One can see from Fig. 4 that although the sample focusing position is the same for all three situations considered the resulting width of the sample is the smaller the steeper the potential gradient, which obviously results in better focusing. In the case of Fig. 4 this had to be achieved by simultaneous increase in both the hydrodynamic flow rate and the electric potential applied along the channel. On the other hand, the same effect can be achieved by changing the geometry of the ion-conducting membrane, viz., by varying the electric field profile without changing the applied potential difference (see Fig. 2). This is exemplified in Fig. 5 for three wedge-shaped membranes with different slopes. It follows that the width of the focused sample depends on the diffusivity of the analyte as well as on the electric field strength. In order to achieve better focusing, the latter can be increased not only via increasing the potential difference applied along the separation channel but also by changing the shape of the ion-conducting membrane. This may allow achieving the same focusing quality using lower voltages than those used for illustration in Figs. 4–5 if this is desired experimentally. On the other hand, it should be noted that employing higher voltages and higher solution flow rates allow the reduction of focusing times which may be advantageous in experimental practice. The plots in Figs. 3–5 evidence the great versatility of the method since they demonstrate that one can adjust the electrical and hydrodynamic conditions to obtain a desired result.

### 3.2 Separation of two differently charged species

If the sample consists of molecules carrying different electric charges and/or different diffusion coefficients each component will be focused at different positions along the channel. Figure 6 illustrates the limiting distribution of two species with  $z = 1$  and  $z = 2$  (and an identical diffusion coefficient for simplicity) for the dimensionless parameters:  $Pe = 100$ ,  $\Psi = 3892.2$ ,  $k = 5$ . The initial samples of the species were superimposed and had the same dimensionless width  $W_s = 1$  as well as equal concentrations. However,

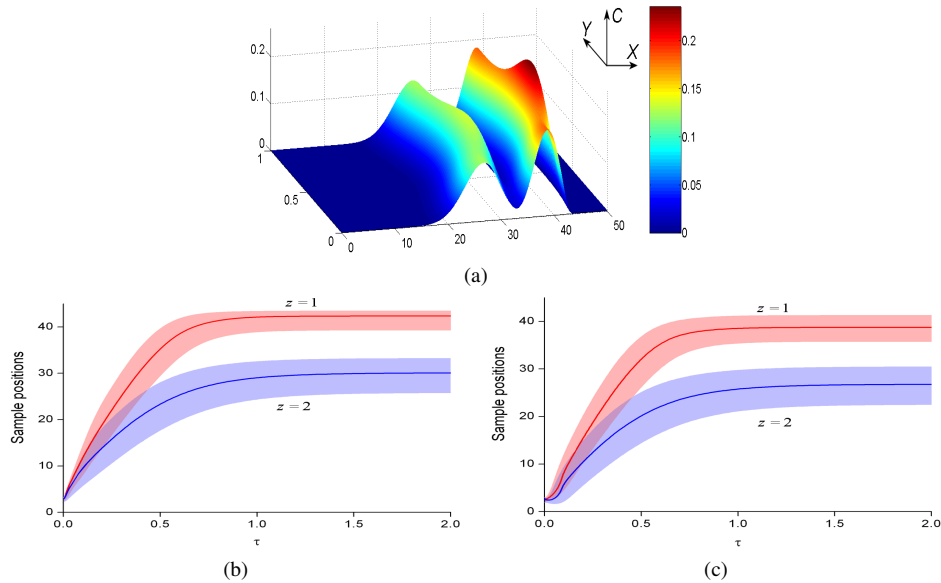


Fig. 6. (a) 3D-representation of the simultaneous focusing of 2 species with  $z = 1$  (peak on the right) and  $z = 2$  (peak on the left), respectively; (b,c) variations of the positions of the two sample maxima in the center ((b)  $Y = 0.5$ ) and near the bottom ((c)  $Y = 0$ ) of the channel as a function of time:  $z = 1$  and  $z = 2$ . The shaded areas around each curve filled with the same color represent the widths of each sample during the focusing operation. See text for other parameter values.

as evidenced in Fig. 6, when focused, the two samples concentration distributions have different amplitudes and widths since they traveled different lengths and are ultimately trapped in areas with different electric field strength (see, e.g., Fig. 2 for  $k = 5$ ).

#### 4 Computational details

A computer program for the numerical solution of the model (16)–(20) was developed by the authors. The time-dependent PDE (19) was solved using the Alternating Direction Implicit finite difference method [71] which affords extremely rapid and accurate simulations. The computer program features a user-friendly interface allowing easy parameter input and graphical presentation of the computed concentration distributions as well as dynamic sample parameters (position and width). The program can be obtained from the authors upon request.

#### 5 Conclusions

This theoretical work based on the concept recently introduced by some of us demonstrates that the focusing of selected analytes in microfluidic separation channels thanks

to the opposition between a constant transport by the hydrodynamic flow and a gradient of the electrophoretic driving force provides extremely interesting opportunities for chemical and biochemical separations. Beyond its high experimental simplicity, the main advantage of this concept is that the key electrical gradient is directly provided by that of the thickness of an ion-conducting membrane so that the system may be optimized for specific analytes of interest by very simple operations. As proven by the theory presented in this work and the corresponding simulations the method is then highly versatile in the sense that these theoretical analyses showed that specific shapes of the ion-conduction membrane thickness profile may ensure the simultaneous focusing of several selected analytes at the same time, a property which may be extremely useful when searching for example for a specific protein distribution pattern in biological fluids.

### Acknowledgements

This work was supported in parts by CNRS (UMR 8640 "PASTEUR" and LIA "Xi-amENS"), Ecole Normale Supérieure (ENS), Université Pierre et Marie Curie (UPMC), the French Ministry of Research and by the NSF of China (No. 20620130427) and MOST of China (No. 2007DFC40440), both funds being related to "International Scientific and Technological Cooperation Projects". Irina Svir thanks ANR Chaire d'Excellence "Micro-NanoChem" (ANR-10-CHEX-012-01) for the financial support of this work.

### References

1. C.T. Culbertson, S.C. Jacobson, J.M. Ramsey, Microchip devices for high-efficiency separations, *Anal. Chem.*, **72**, pp. 5814–5819, 2000.
2. P.S. Dittrich, K. Tachikawa, A. Manz, Micro total analysis systems. Latest advancements and trends, *Anal. Chem.*, **78**, pp. 3887–3907, 2006.
3. J.W. Zhou, A.V. Ellis, N.H. Voelcker, Recent developments in PDMS surface modification for microfluidic devices, *Electrophoresis*, **31**, pp. 2–16, 2010.
4. S.C. Jacobson, J.M. Ramsey, Microfabricated Chemical Separation Devices, in: M.G. Khaledi (Ed.), *High-Performance Capillary Electrophoresis*, Vol. 146, J. Wiley & Sons, New York, 1988, pp. 613–633.
5. D.R. Reyes, D. Iossifidis, P.-A. Auroux, A. Manz, Micro total analysis systems. 1. Introduction, theory, and technology, *Anal. Chem.*, **74**, pp. 2623–2636, 2002.
6. P.-A. Auroux, D. Iossifidis, D.R. Reyes, A. Manz, Micro total analysis systems. 2. Analytical standard operations and applications, *Anal. Chem.*, **74**, pp. 2637–2652, 2002.
7. T. Vilckner, D. Janasek, A. Manz, Micro total analysis systems. Recent developments, *Anal. Chem.*, **76**, pp. 3373–3386, 2004.
8. P.S. Dittrich, K. Tachikawa, A. Manz, Micro total analysis systems. Latest advancements and trends, *Anal. Chem.*, **78**, pp. 3887–3908, 2006.

9. J. West, M. Becker, S. Tombrink, A. Manz, Micro total analysis systems: Latest achievements, *Anal. Chem.*, **80**, pp. 4403–4419, 2008.
10. A. Arora, G. Simone, G.B. Salieb-Beugelaar, J.T. Kim, A. Manz, Latest developments in micro total analysis systems, *Anal. Chem.*, **82**, pp. 4830–4847, 2010.
11. G.B. Salieb-Beugelaar, G. Simone, A. Arora, A. Philippi, A. Manz, Latest developments in microfluidic cell biology and analysis systems, *Anal. Chem.*, **82**, pp. 4848–4864, 2010.
12. D.J. Harrison, A. Manz, Z. Fan, H. Luedi, H.M. Widmer, Capillary electrophoresis and sample injection systems integrated on a planar glass chip, *Anal. Chem.*, **64**, pp. 1926–1932, 1992.
13. C.S. Effenhauser, A. Manz, H.M. Widmer, Glass chips for high-speed capillary electrophoresis separations with submicrometer plate heights, *Anal. Chem.*, **65**, pp. 2637–2642, 1993.
14. S.C. Jacobson, C.T. Culbertson, J.E. Daler, J.M. Ramsey, Microchip structures for submillisecond electrophoresis, *Anal. Chem.*, **70**, pp. 3476–3480, 1998.
15. J.S. Mecomber, A.M. Stalcup, D. Hurd, H.B. Halsall, W.R. Heineman, C.J. Seliskar, K.R. Wehmeyer, P.A. Limbach, Analytical performance of polymer-based microfluidic devices fabricated by computer numerical controlled machining, *Anal. Chem.*, **78**, pp. 936–941, 2006.
16. J.G. Shackman, M.S. Munson, D. Ross, Gradient elution moving boundary electrophoresis for high-throughput multiplexed microfluidic devices, *Anal. Chem.*, **79**, pp. 565–571, 2007.
17. C.S. Effenhauser, G.J.M. Bruin, A. Paulus, Integrated chip-based capillary electrophoresis, *Electrophoresis*, **18**, pp. 2203–2213, 1997.
18. J.P. Kutter, S.C. Jacobson, J.M. Ramsey, Integrated microchip device with electrokinetically controlled solvent mixing for isocratic and gradient elution in micellar electrokinetic chromatography, *Anal. Chem.*, **69**, pp. 5165–5171, 1997.
19. A.W. Moore, Jr., S.C. Jacobson, J.M. Ramsey, Microchip separations of neutral species via micellar electrokinetic capillary chromatography, *Anal. Chem.*, **67**, pp. 4184–4189, 1995.
20. J.P. Kutter, S.C. Jacobson, N. Matsubara, J.M. Ramsey, Solvent-programmed microchip open-channel electrochromatography, *Anal. Chem.*, **70**, pp. 3291–3297, 1998.
21. R. Wu, H. Zou, M. Ye, Z. Lei, J. Ni, Capillary electrochromatography for separation of peptides driven with electrophoretic mobility on monolithic column, *Anal. Chem.*, **73**, pp. 4918–4923, 2001.
22. R. Xiang, C. Horvath, Fundamentals of capillary electrochromatography: Migration behavior of ionized sample components, *Anal. Chem.*, **74**, pp. 762–770, 2002.
23. P.C. Simpson, D. Roach, A.T. Woolley, T. Thorsen, R. Johnston, G.F. Sensabaugh, R.A. Mathies, High-throughput genetic analysis using microfabricated 96-sample capillary array electrophoresis microplates, *Proc. Natl. Acad. Sci. USA*, **95**, pp. 2256–2261, 1998.
24. C.S. Effenhauser, A. Paulus, A. Manz, H.M. Widmer, High-speed separation of antisense oligonucleotides on a micromachined capillary electrophoresis device, *Anal. Chem.*, **66**, pp. 2949–2953, 1994.

25. A.T. Woolley, R.A. Mathies, Ultra-high-speed DNA fragment separations using microfabricated capillary array electrophoresis chips, *Proc. Natl. Acad. Sci. USA*, **91**, pp. 11348–11352, 1994.
26. L.C. Waters, S.C. Jacobson, N. Kroutchinina, J. Khandurina, R.S. Foote, J.M. Ramsey, Microchip device for cell lysis, multiplex PCR amplification, and electrophoretic sizing, *Anal. Chem.*, **70**, pp. 158–162, 1998.
27. Z. Zhuang, J.A. Starkey, Y. Mechref, M.V. Novotny, S.C. Jacobson, Electrophoretic analysis of *N*-glycans on microfluidic devices, *Anal. Chem.*, **79**, pp. 7170–7175, 2007.
28. C. Hou, A.E. Herr, Ultrashort separation length homogeneous electrophoretic immunoassays using on-chip discontinuous polyacrylamide gels, *Anal. Chem.*, **82**, pp. 3343–3351, 2010.
29. D. Ross, E.F. Romantseva, Gradient elution moving boundary electrophoresis with channel current detection, *Anal. Chem.*, **81**, pp. 7326–7335, 2009.
30. N. Hu, J. Yang, Z.-Q. Yin, Y. Ai, S. Qian, I. Svir, B. Xia, J.-W. Yan, W.-S. Hou, X.-L. Zheng, A high-throughput dielectrophoresis-based cell electrofusion microfluidic device, *Electrophoresis*, **32**, pp. 2488–2495, 2011.
31. J. Yang, L.-P. Zhao, Z.-Q. Yin, N. Hu, J. Chen, T.-Y. Li, I. Svir, X.-L. Zheng, Chip-based cell electrofusion, *Adv. Eng. Mater.*, **12**(9), pp. B398–B405, 2010.
32. J.R. Yates 3rd., Mass spectrometry: From genomics to proteomics, *Trends Genet.*, **16**, pp. 5–8, 2000.
33. R. Aebersold, M. Mann, Mass spectrometry-based proteomics, *Nature*, **422**, pp. 198–207, 2003.
34. S. Naylor, R. Kumar, Emerging role of mass spectrometry in structural and functional proteomics, *Adv. Protein Chem.*, **65**, pp. 217–248, 2003.
35. P. Jolles, H. Jornvall (Eds.), *Proteomics in Functional Genomics: Protein Structure Analysis*, Birkhauser, Basel, 2000.
36. J.C. Tran, A.A. Doucette, Gel-eluted liquid fraction entrapment electrophoresis: An electrophoretic method for broad molecular weight range proteome separation, *Anal. Chem.*, **80**, pp. 1568–1573, 2008.
37. J.S. Mellors, K. Jorabchi, L.M. Smith, J.M. Ramsey, Integrated microfluidic device for automated single cell analysis using electrophoretic separation and electrospray ionization mass spectrometry, *Anal. Chem.*, **82**, pp. 967–973, 2009.
38. Z.-W. Tian, H.S. Lin, Y.L. Zhou, Electrophoretic separating device and method for using the device, European Patent, WO0235223 (applied: October 25, 2000; authorized: January 18, 2006).
39. Z.-W. Tian, D.Y. Chen, H.S. Lin, Counter flow focusing electrophoresis device and method for using the device, Chinese Patent, 98104828.5 (applied: January 15, 1998; authorized: June 28, 2001) (in Chinese).

40. Q. Wang, S.L. Lin, K.F. Warnick, D.H. Tolley, M.L. Lee, Voltage-controlled separation of proteins by electromobility focusing in a dialysis hollow fiber, *J. Chromatography A*, **985**, pp. 455–462, 2003.
41. P. Myers, K.D. Bartle, Towards a miniaturised system for dynamic field gradient focused separation of proteins, *J. Chromatography A*, **1044**, pp. 253–258, 2004.
42. J.G. Shackman, D. Ross, Counter-flow gradient electrofocusing, *Electrophoresis*, **28**, pp. 556–571, 2007.
43. K.F. Warnick, S.J. Francom, P.H. Humble, R.T. Kelly, A.T. Woolley, M.L. Lee, H.D. Tolley, Field gradient electrophoresis, *Electrophoresis*, **26**, pp. 405–414, 2005.
44. S.L. Lin, H.D. Tolley, M.L. Lee, Voltage-controlled electric field gradient focusing with online UV detection for analysis of proteins, *Chromatographia*, **62**, pp. 277–281, 2005.
45. G. Danger, D. Ross, Development of a temperature gradient focusing method for in situ extraterrestrial biomarker analysis, *Electrophoresis*, **29**, pp. 3107–3114, 2008.
46. B.O. Eriksson, M. Dahl, M.B.O. Andersson, L.G. Blomberg, Changes in mobile phase ion distribution when combining pressurized flow and electric field, *Electrophoresis*, **25**, pp. 3092–3097, 2004.
47. V. Kostal, B.R. Fonslow, E.A. Arriaga, M.T. Bowser, Fast determination of mitochondria electrophoretic mobility using micro free-flow electrophoresis, *Anal. Chem.*, **81**, pp. 9267–9273, 2009.
48. P.H. O'Farrell, Separation techniques based on the opposition of two counteracting forces to produce a dynamic equilibrium, *Science*, **227**, pp. 1586–1589, 1985.
49. W.S. Koegler, C.F. Ivory, Focusing proteins in an electric field gradient, *J. Chromatography A*, **726**, pp. 229–236, 1996.
50. H.C. Cui, K. Horiuchi, P. Dutta, C.F. Ivory, Multistage isoelectric focusing in a polymeric microfluidic chip, *Anal. Chem.*, **77**, pp. 7878–7886, 2005.
51. J.G. Shackman, D. Ross, Gradient elution isotachopheresis for enrichment and separation of biomolecules, *Anal. Chem.*, **79**, pp. 6641–6649, 2007.
52. D. Kohlheyer, J.C.T. Eijkel, S. Schlautmann, A. van den Berg, R.B.M. Schasfoort, Microfluidic high-resolution free-flow isoelectric focusing, *Anal. Chem.*, **79**, pp. 8190–8198, 2007.
53. J.W. Albrecth, J. El-Ali, K.F. Jensen, Cascaded free-flow isoelectric focusing for improved focusing speed and resolution, *Anal. Chem.*, **79**, pp. 9364–9371, 2007.
54. G.J. Sommer, A.K. Singh, A.V. Hatch, On-chip isoelectric focusing using photopolymerized immobilized pH gradients, *Anal. Chem.*, **80**, pp. 3327–3333, 2008.
55. K. Shimura, K. Takahashi, Y. Koyama, K. Sato, T. Kitamori, Isoelectric focusing in a microfluidically defined electrophoresis channel, *Anal. Chem.*, **80**, pp. 3818–3823, 2008.
56. N.I. Davis, M. Mamunooru, C.A. Vyas, J.G. Shackman, Capillary and microfluidic gradient elution isotachopheresis coupled to capillary zone electrophoresis for femtomolar amino acid detection limits, *Anal. Chem.*, **81**, pp. 5452–5459, 2009.

57. E.A. Strychalski, A.C. Henry, D. Ross, Microfluidic analysis of complex samples with minimal sample preparation using gradient elution moving boundary electrophoresis, *Anal. Chem.*, **81**, pp. 10201–10207, 2009.
58. A.J. Hughes, A.J. Herr, Quantitative enzyme activity determination with zeptomole sensitivity by microfluidic gradient-gel zymography, *Anal. Chem.*, **82**, pp. 3803–3811, 2010.
59. M.B. Kerby, M. Spaid, S. Wu, J.W. Parce, R.L. Chien, Selective ion extraction: separation method for microfluidic devices, *Anal. Chem.*, **74**, pp. 5175–5183, 2002.
60. W.N. Vreeland, S.J. Williams, A.E. Barron, A.P. Sassi, Tandem isotachopheresis-zone electrophoresis via base-mediated destacking for increased detection sensitivity in microfluidic systems, *Anal. Chem.*, **75**, pp. 3059–3065, 2003.
61. R. Dhopeswarkar, D. Hlushkou, M. Nguyen, U. Tallarek, R.M. Crooks, Electrokinetics in microfluidic channels containing a floating electrode, *J. Am. Chem. Soc.*, **130**, pp. 10480–10481, 2008.
62. D.R. Laws, D. Hlushkou, R.K. Perdue, U. Tallarek, R.M. Crooks, Bipolar electrode focusing: Simultaneous concentration enrichment and separation in a microfluidic channel containing a bipolar electrode, *Anal. Chem.*, **81**, pp. 8923–8929, 2009.
63. D. Hlushkou, R.K. Perdue, R. Dhopeswarkar, R.M. Crooks, U. Tallarek, Electric field gradient focusing in microchannels with embedded bipolar electrode, *Lab Chip*, **9**, pp. 1903–1913, 2009.
64. R.K. Perdue, D.R. Laws, D. Hlushkou, U. Tallarek, R.M. Crooks, Bipolar electrode focusing: The effect of current and electric field on concentration enrichment, *Anal. Chem.*, **81**, pp. 10149–10155, 2009.
65. J.P. Hsu, Z.S. Chen, S. Tseng, Effect of electroosmotic flow on the electrophoresis of a membrane-coated sphere along the axis of a cylindrical pore, *J. Phys. Chem. B*, **113**, pp. 7701–7708, 2009.
66. S. Das, S. Chakraborty, Transport and separation of charged macromolecules under nonlinear electromigration in nanochannels, *Langmuir*, **24**, pp. 7704–7710, 2008.
67. S. Das, S. Chakraborty, Influence of streaming potential on the transport and separation of charged spherical solutes in nanochannels subjected to particle-wall interactions, *Langmuir*, **25**, pp. 9863–9872, 2009.
68. W. Thormann, M.C. Breadmore, J. Caslavská, R.A. Mosher, Dynamic computer simulations of electrophoresis: A versatile research and teaching tool, *Electrophoresis*, **31**, pp. 726–754, 2010.
69. G. Bruhat, *Cours de Physique Générale: Electricité*, 8th edition, Masson & Cie, Paris, 1967, pp. 235–236.
70. A.J. Bard, L.R. Faulkner, *Electrochemical Methods: Fundamentals and Applications*, 2nd edition, J. Wiley & Sons, New York, 2001, pp. 138–139.
71. W.H. Press, S.A. Teukolsky, W.T. Vetterling, B.P. Flannery, *Numerical Recipes: The Art of Scientific Computing*, 3rd edition, Cambridge Univ. Press, New York, 2007.